CrossMark

LETTER

Electrical, Thermal and Spectroscopic Characterization of Bulk Bi_2Se_3 Topological Insulator

Rabia Sultana[1,2] · Geet Awana[1,3] · Banabir Pal[4] · P. K. Maheshwari[1,2] ·
Monu Mishra[1,2] · Govind Gupta[1,2] · Anurag Gupta[1,2] · S. Thirupathaiah[4] ·
V. P. S. Awana[1,2]

Abstract We report the electrical (angular magneto-resistance and Hall), thermal (heat capacity) and spectroscopic (Raman, X-ray photoelectron, angle-resolved photoelectron) characterization of a bulk Bi_2Se_3 topological insulator, which was grown by self-flux method through solid-state reaction from high-temperature (950 °C) melt and slow cooling (2 °C/h) of constituent elements. Bi_2Se_3 exhibited metallic behaviour down to 5 K. Magneto-transport measurements revealed linear up to 400 and 30% magneto-resistance (MR) at 5 K under a 14-T field in perpendicular and parallel field directions, respectively. We noticed that the MR of Bi_2Se_3 is very sensitive to the angle of the applied field. The MR is maximum when the field is normal to the sample surface, while it is minimum when the field is parallel. The Hall coefficient (R_H) is seen nearly invariant with a negative carrier sign down to 5 K albeit having near-periodic oscillations above 100 K. The heat capacity (C_p) versus temperature plot is seen without any phase transitions down to 5 K and is well fitted ($C_p = \gamma T + \beta T^3$) at low temperature with a calculated Debye

temperature (θ_D) value of 105.5 K. Clear Raman peaks are seen at 72, 131 and 177 cm^{-1} corresponding to A_{1g}^1, E_g^2 and A_{1g}^2, respectively. Though two distinct asymmetric characteristic peak shapes are seen for Bi $4f_{7/2}$ and Bi $4f_{5/2}$, the Se 3d region is found to be broad, displaying the overlapping of spin-orbit components of the same. Angle-resolved photoemission spectroscopy (ARPES) data of Bi_2Se_3 revealed distinctly the bulk conduction bands (BCB), surface state (SS), Dirac point (DP) and bulk valence bands (BVB), and 3D bulk conduction signatures are clearly seen. Summarily, a host of physical properties for the as-grown Bi_2Se_3 crystal are reported here.

1 Introduction

Topological insulators (TIs) are among one of the most challenging hot topics today in condensed matter physics. In fact, the ongoing vast field of research leading to the discovery of some interesting TIs (Bi_2Se_3, Bi_2Te_3 and Sb_2Te_3) with unique properties and application potential had attracted much attention of condensed matter physicists worldwide [1–6]. TIs are like an ordinary insulator in the interior and conducting on the outside surface/edges. This dual nature, i.e. insulating as well as conducting, occurs due to the presence of bulk band gap in the interior and topologically protected conducting states on the surface. The topological surface states in three-dimensional (3D) TIs have been predominantly examined by angle-resolved photoemission spectroscopy (ARPES), scanning tunnelling microscopy (STM) and band structure calculations [7–10]. The topologically protected conducting states in TIs arise due to the strong spin-orbit interaction (SOI) and time

✉ V. P. S. Awana
awana@nplindia.org
awanavps.webs.com

1 National Physical Laboratory (CSIR), Dr. K. S. Krishnan Road, New Delhi 110012, India

2 Academy of Scientific and Innovative Research, NPL, New Delhi 110012, India

3 Department of Physics and Astrophysics, Delhi University, New Delhi 110007, India

4 Solid State and Structural Chemistry Unit, Indian Institute of Science, Bangalore, Karnataka 560012, India

reversal symmetry (TRI). TIs could be useful from the application point of view as spintronic and quantum computation devices [1]. Interestingly, TIs also behave as superconductors when intercalated or doped with elements like Sr, Cu, Nb and Tl [11–17].

Apparently, Bi_2Se_3 and Bi_2Te_3 are among the most studied bulk TI compounds [1–10], which crystallize in a rhombohedral structure belonging to the $R\bar{3}m$ (D5) space group. It is well known that these bulk 3D TIs exhibit a gapless single Dirac cone on the surface coupled with strong SOI and a large bulk energy gap of 0.3 eV between the bulk bands [7–9]. Further, Bi_2Se_3 is a pure compound rather than an alloy like Bi_xSb_{1-x}, and the presence of a relatively large bulk energy gap of 0.3 eV holds promises for room-temperature applications [10, 19, 20]. It is also known that Bi_2Se_3 exhibits a high thermoelectric figure of merit (ZT) for commercial applications [18]. The linear magneto-resistance (MR) as well as the angular-dependent MR behaviour is observed in thin films, nano-plates, nanowires/nano-ribbons, nano-sheets and crystals of different TIs like Bi_2Te_3 and Bi_2Se_3 [19, 21–24]. Accordingly, Bi_2Se_3 is thought to be a promising TI system toward unique applications for next-generation spintronics, quantum computation and optoelectronics.

In the present study, we investigate the synthesis as well as characterization of a bulk Bi_2Se_3 TI. A host of physical property characterizations including angular magneto-transport, heat capacity and Hall measurement along with various spectroscopic studies, viz. Raman, photoelectron and angle-resolved photoelectron, are reported here for the as-grown Bi_2Se_3 TI.

2 Experimental Details

High-quality bulk Bi_2Se_3 single crystal has been synthesized by self-flux method through the conventional solid-state reaction route [25, 26]. High-purity (99.99%) bismuth (Bi) and selenium (Se) were used as the starting materials. Stoichiometric amounts of the starting materials were accurately weighed, well mixed and ground thoroughly inside a glove box (MBRAUN LABstar) under high-purity Ar atmosphere to avoid oxidation of the sample. The homogeneously mixed powder was pressed into a rectangular pellet using a hydraulic press under a pressure of 50 kg/cm^2 and then sealed into an evacuated (10^{-3} Torr) quartz tube. The vacuum-encapsulated quartz tube was then sintered inside a tube furnace with a step increase rate of 2 °C/min up to 950 °C, kept there for 12 h and then slowly cooled down to 650 °C at a rate of 2 °C/h. Further, the furnace was switched off and allowed to cool to room temperature. Figure 1 shows the schematic heat treatment diagram. The resultant sample was taken out by breaking the quart tube carefully. The obtained sample was shiny and silver in colour, which was
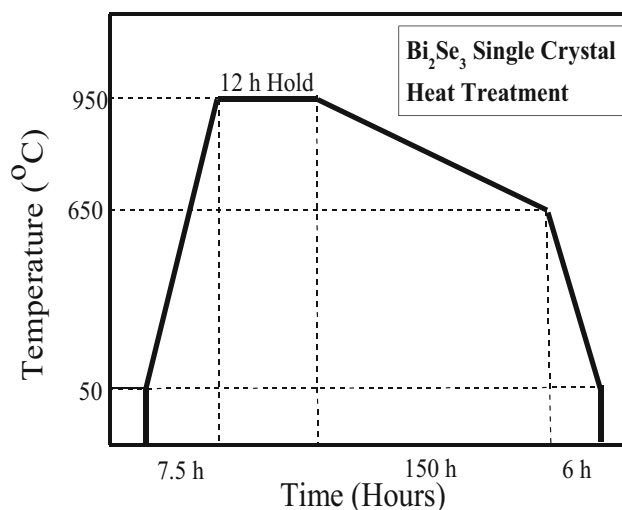

Fig. 1 Schematic diagram of heat treatment to grow bulk Bi_2Se_3 single crystal

mechanically cleaved for further measurements. Characterizations of the synthesized Bi_2Se_3 crystal were performed using X-ray diffraction (XRD), Raman spectroscopy, scanning electron microscopy (SEM) and X-ray photoelectron spectroscopy (XPS). Further, magnetic and resistivity measurements under magnetic field were carried out by a conventional four-probe method on a Quantum Design Physical Property Measurement System (PPMS) with fields up to 14 T.

3 Results and Discussion

To examine the crystallographic structure, chemical composition and lattice parameters of the obtained sample, room-temperature X-ray diffraction (XRD) was performed using a Rigaku MiniFlex-II X-ray diffractometer with Cu-Kα radiation ($\lambda = 1.5418$ Å). Figure 2a shows the Rietveld-fitted room-temperature XRD pattern of the studied gently powdered bulk Bi_2Se_3 single crystal performed using the FullProf Suite toolbar. The compound is crystallized in a rhombohedral structure within the $R\bar{3}m$ (D5) space group. Apparently, the studied sample exhibits a single phase without any impurities within the XRD limits. The lattice parameters are $a = b \neq c$, and their corresponding values are $a = b = 4.14(2)$ Å and $c = 28.701(3)$ Å, respectively. The inset of Fig. 2a shows the single-crystal XRD pattern from the surface of the as-obtained bulk Bi_2Se_3 crystal with 00l planes being aligned along one direction. It is clear from the inset of Fig. 2a that the obtained crystal is textured and grew along the c-direction.

Figure 2b shows the unit cell structure of the studied bulk Bi_2Se_3 single crystal as being formed and analysed by the VESTA software from the Rietveld-refined lattice parameters and the atomic positions. The studied Bi_2Se_3 crystal
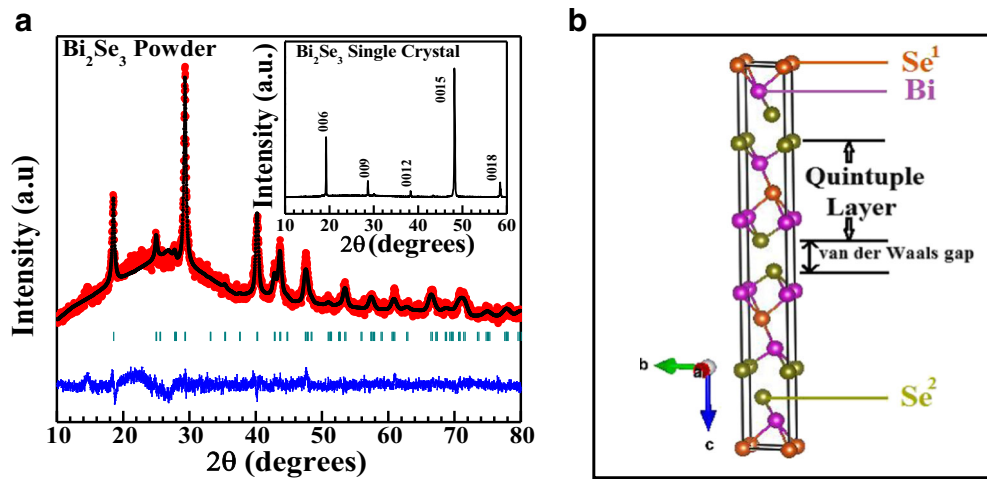
Fig. 2 **a** Rietveld-fitted room-temperature X-ray diffraction pattern for powder Bi_2Se_3 crystal. *Inset* represents X-ray diffraction pattern for Bi_2Se_3 single crystal. **b** Unit cell structure of Bi_2Se_3 single crystal

exhibits a rhombohedral structure composed of three quintuple layers (QLs) stacked one over the other. As reported earlier, each QL arranged as Se-Bi-Se-Bi-Se is separated by weak van der Waals force [1–6, 26]. Noticeably, this weak van der Waals force makes the QL to slide over each other similar to graphite and helps the single crystal to cleave easily.

The morphological characteristics as well as the chemical composition of the synthesized Bi_2Se_3 single crystal were analysed by scanning electron microscopy (SEM) and energy-dispersive X-ray spectroscopy (EDAX). The SEM image of the resultant bulk Bi_2Se_3 single crystal exhibited layered (00l) directional growth, and the quantitative weight% of the atomic constituents (Bi and Se) was found to be near the stoichiometric amount. Apparently, the studied crystal is pure (uncontaminated from impurities like carbon or oxygen), composed of atomic constituents Bi and Se; details are reported by some of us in an earlier short article [25]. The temperature versus resistivity of the studied Bi_2Se_3 sample with and without various applied magnetic fields exhibited metallic behaviour down to 2 K. Here, the field was applied in a direction perpendicular to the

current flow. Accordingly, the $\rho(T)H$ plots exhibited metallic behaviour having positive temperature coefficient values [25].

Figure 3a, b displays the percentage change of magnetoresistance $MR = [\rho(H) - \rho(0)]/\rho(0)$ as a function of applied magnetic field [$H \perp c$-axis ($\theta = 0°$) and $H // c$-axis ($\theta = 90°$)] up to 14 T at different temperatures (from 5 to 200 K). Under perpendicular applied magnetic field ($\theta = 0°$) up to 14 T, the studied Bi_2Se_3 crystal exhibits a linear positive MR value increasing from 60% at 200 K to 400% at 5 K (Fig. 3a). However, under parallel applied magnetic field ($\theta = 90°$), the MR value of the studied sample decreases from 30% at 5 K to 6% at 200 K (Fig. 3b). Clearly, the MR is decreased by an order of magnitude in parallel applied magnetic field. Accordingly, we can say that the studied sample exhibited the largest, high-field non-saturating positive MR (%) value reaching up to 400% at 5 K, when measured under perpendicular magnetic field. The high value of MR (400%) seems interesting both from the basic research and from the application point of view. Thus, we observed a giant linear MR effect sensitive to the applied magnetic field (H)
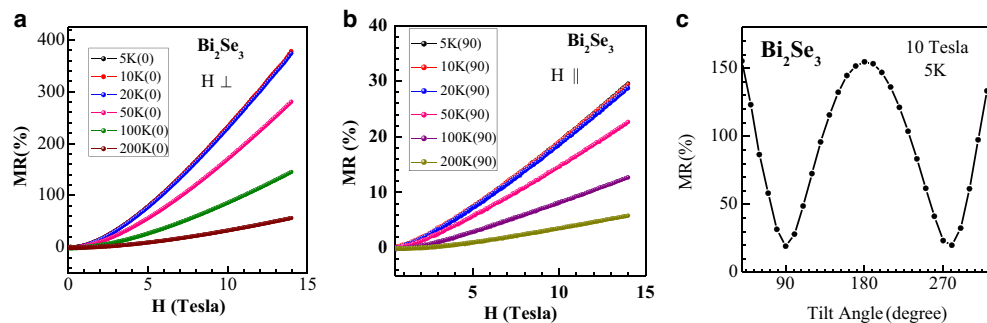

Fig. 3 **a** MR (%) as a function of magnetic field perpendicular to *ab* plane for Bi_2Se_3 at different temperatures. **b** MR (%) as a function of magnetic field parallel to *ab* plane for Bi_2Se_3 at different temperatures. **c** Angular dependence of MR for Bi_2Se_3 at 5 K under 10-T applied field
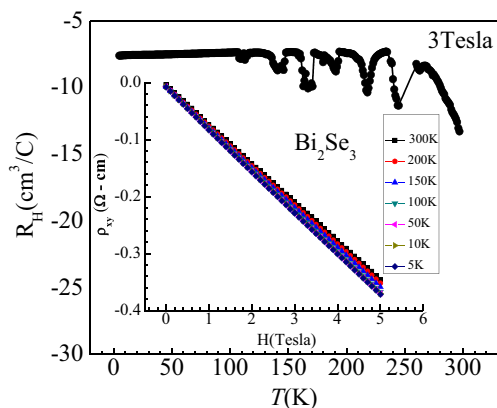
Fig. 4 Hall coefficient (R_H) as a function of temperature (T) at constant magnetic field of 3 T; the *inset* shows the Hall resistivity (ρ_{xy}) versus magnetic field (up to 5 T) plot at different temperatures from 330 to 5 K of the studied Bi_2Se_3 crystal

direction, which is maximum for perpendicular and least for parallel field.

Figure 3c represents the percentage change of magneto-resistance MR $= [\rho(H) - \rho(0)]/\rho(0)$ as a function of rotation angle (θ) under constant applied magnetic field and temperature of 10 T and 5 K, respectively. The peak is observed at $\theta° =° 180°$ (perpendicular magnetic field), while the dips are seen at $\theta = 90°$ and $\theta° =° 270°$ (parallel magnetic field). Thus, we can say that the resultant Bi_2Se_3 crystal has a unique response to the perpendicular component of magnetic field at different tilt angles, confirming the linear MR as a 2D magneto-transport effect as reported earlier [19].

Figure 4 displays the Hall coefficient (R_H) as a function of temperature (T) at constant magnetic field of 3 T. The R_H is observed to increase with decreasing temperature down to 100 K along with exhibiting harmonic oscillations. Below 100 K, the curve tends to saturate. The inset of Fig. 4 shows the Hall resistivity (ρ_{xy}) versus magnetic field (up to
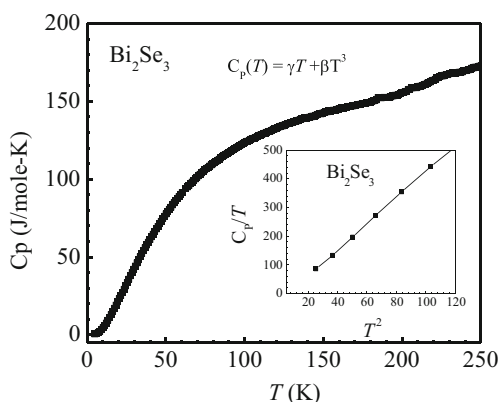
5 T) plot at different temperatures from 330 to 5 K of the studied Bi_2Se_3 crystal. Two pieces of important information drawn from Fig. 4 and its inset are that the R_H is nearly invariant with temperature in the range of 5 to 300 K albeit with the near-periodic oscillation above 100 K and that the carrier sign is negative in the studied temperature range. In-depth studies are underway to understand the R_H behaviour, particularly above 100 K.

Figure 5 displays the heat capacity (C_p) versus temperature (C_p-T) plot for the studied Bi_2Se_3 crystal in the temperature range of 250 down to 5 K. The C_p value increases with increase in temperature but eventually saturates at higher temperature. The inset of Fig. 5 represents the C_p/T versus T^2 plot of the studied crystal. Here, the C_p is calculated using the formula $C_p = \gamma T + \beta T^3$, where γ and β represent the coefficients of Sommerfeld and phononic contribution, respectively. The Debye temperature (θ_D) value comes out to be 105.5 K, calculated using the equation $\theta_D = [12\pi^4 N_A z k_B/5\beta]^{1/3}$, where N_A represents Avogadro's constant, z is the number of atoms per formula unit and k_B is Boltzmann's constant. The nature of both the graphs is in agreement with the previously reported Sb_2Te_3 single crystal [27]. However, the intercept γ crosses near the zero value. The reason may be that we measured C_p down to 5 K only, which had been measured and fitted down to 2 K in [27]. Nonetheless, the shape of the C_p plot is identical to that reported in [27], and the values thus obtained are comparable.

To observe the vibrational modes of the studied Bi_2Se_3, Raman spectroscopy of the synthesized crystal was recorded using the Renishaw Raman spectrometer. Figure 6 shows the Raman spectra of the bulk Bi_2Se_3 single crystal recorded at room temperature. According to group theory, the irreducible representation for the zone centre phonon can be illustrated as $\Gamma = 2E_g + 2A_{1g} + 2E_u + 2A_{1u}$, where g and u represents the gerade (Raman-active modes: $2E_g$, $2A_{1g}$) and ungerade (infrared-active modes: $2E_u$, $2A_{1u}$) modes, respectively [28–30]. Figure 6 clearly shows three distinct
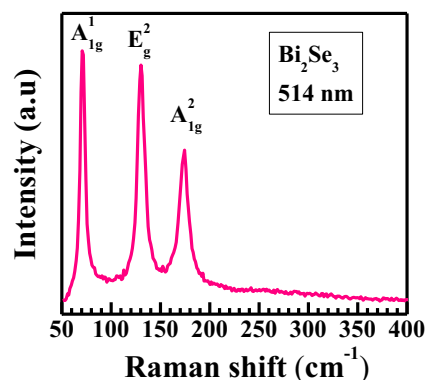

Fig. 5 Temperature dependence of the heat capacity (C_p) of Bi_2Se_3 single crystal. *Inset* shows the C_p/T versus T^2 plot of the studied crystal

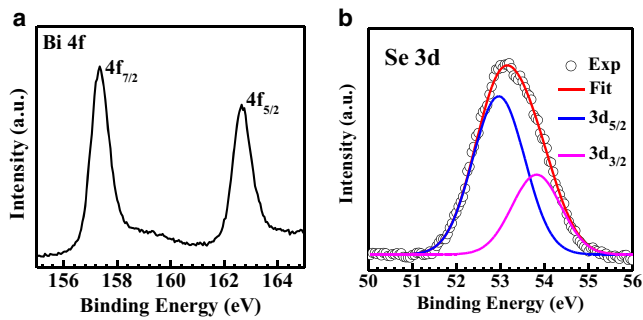**Fig. 6** Raman spectra for Bi_2Se_3 single crystal at room temperature

Fig. 7 X-ray photoelectron spectroscopy (XPS) for studied Bi_2Se_3 single crystal. **a** Bi 4f. **b** Se 3d

Raman-active modes at 72, 131 and 177 cm^{-1} corresponding to A_{1g}^1, E_g^2 and A_{1g}^2, respectively. These values are in good agreement with the earlier reported results and affirm that the crystals are of good quality [29, 30]. Consequently, we can say that these peaks are shifted to a higher frequency in comparison to the reported Bi_2Te_3 [26]. Interestingly, the other (E_{1g}^1) lowest frequency Raman-active mode is not observed, which is similar to most of the earlier reported literature [31, 32].

Further, to examine the surface chemistry of the studied Bi_2Se_3 single crystal, X-ray photoelectron spectroscopy (XPS) was employed using the Omicron multi-probe surface analysis system equipped with a monochromatic Al-Kα source having an excitation energy of 1486.7 eV. Figure 7a, b depicts the XPS spectra recorded for the Bi_2Se_3 single crystal. Figure 7a represents the primary XPS region of bismuth (Bi 4f). The Bi 4f region exhibits two distinct asymmetric characteristic peak shapes for Bi $4f_{7/2}$ and Bi $4f_{5/2}$ with corresponding binding energies of 157.4 and 162.8 eV, respectively. Accordingly, the difference in the binding energies appears to be 5.4 eV, revealing the well-separated spin-orbit components of the Bi 4f region. Additionally, a blue shift of 0.4 eV is also shown by the binding energies of Bi 4f peaks with respect to metallic bismuth [32, 33]. Figure 7b displays the primary XPS region of selenium (Se 3d). The observed Se 3d region is found to be broad, and thus, de-convolution was performed to identify the peaks by the Gaussian-Lorentzian function. Two different peaks were observed at Se $3d_{5/2}$ and Se $3d_{3/2}$ with binding energies of 53.0 and 53.8 eV, respectively. Here, the difference in the binding energies is found to be 0.8 eV, displaying the overlapping spin-orbit components of the Se3d peak. Further, the binding energies of Se3d peaks reveal a red shift of about 2.6 eV with respect the Se metal [32, 33]. The elemental composition was calculated using the formula ρ_{Se}/ρ_{Bi}, where ρ is the atomic density. Interestingly, the elemental composition value appears to be 1.27, which is close to the stoichiometric ratio of Bi_2Se_3.

Figure 8 depicts angle-resolved photoemission spectroscopy (ARPES) data of Bi_2Se_3. The measurements were
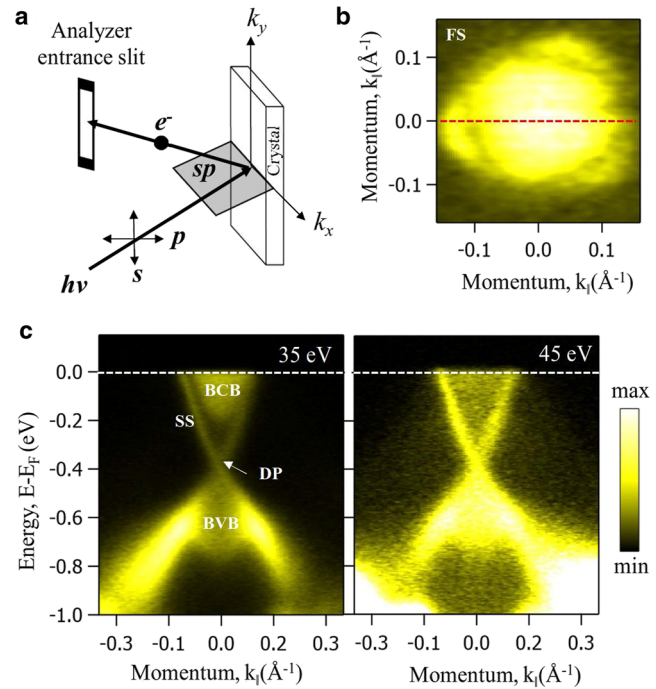

Fig. 8 ARPES of Bi_2Se_3 single crystal. **a** Measuring geometry. **b** Fermi surface map. **c** Energy distribution maps measured along the cut shown in **b** with photon energies 35 and 45 eV. All the data are recorded using *p*-polarized light

performed at the APE beamline in Elettra Synchrotron, Trieste, equipped with a Scienta DA30 deflection analyzer. Figure 8a schematically shows a typical measuring geometry in which *s*- and *p*-plane-polarized lights are defined with respect to the analyzer entrance slit and the scattering plane (SP). Figure 8b depicts Fermi surface (FS) map measured using a photon energy of 35 eV. Figure 8c shows energy distribution maps (EDMs) measured using photon energies of 35 and 45 eV from the left to the right, respectively, along the cut shown by the red dashed line in Fig. 8b. All the data were measured using *p*-polarized light. In the left panel of Fig. 8c, BCB, SS, DP and BVB represent bulk conduction bands, surface state, Dirac point and bulk valence bands, respectively. From the photon energy-dependent EDMs as shown in Fig. 8c, one can clearly notice that the bulk conduction and valance bands are sensitive to the used photon energy, thus suggesting that these are of 3D character. On the other hand, surface states are intact with the varying photon energy. The ARPES results obtained for the studied Bi_2Se_3 crystals are in general agreement with previous reports [4–11].

4 Conclusion

Summarily, in the present article, we reported on the crystal growth, the structure and in brief a host of physical

properties including electrical (angular MR, Hall), thermal (heat capacity) and spectroscopic (Raman, XPS and ARPES) of the Bi_2Se_3 topological insulator.

References

1. Hasan, M.Z., Kane, C.L.: Rev. Mod. Phys. **82**, 3045 (2010)
2. Ando, Y.: J. Phys. Soc. Jpn. **82**, 102001 (2013)
3. Ando, Y., Fu, L.: Annu. Rev. Condens. Matter Phys. **6**, 361 (2015)
4. Fu, L., Kane, C.L., Mele, E.J.: Phys. Rev. Lett. **98**, 106803 (2007)
5. Moore, J.E., Balents, L.: Phys. Rev. B **75**, 121306 (2007)
6. Dai, X., Hughes, T.L., Qi, X.-L., Fang, Z., Zhang, S.-C.: Phys. Rev. B **77**, 125319 (2008)
7. Xia, Y., Qian, D., Hsieh, D., Wray, L., Pal, A., Lin, H., Bansil, A., Grauer, D., Hor, Y.S., Cava, R.J., Hasan, M.Z.: Nat Phys **5**, 398 (2009)
8. Hsieh, D., Xia, Y., Qian, D., Wray, L., Dil, J.H., Meier, F., Osterwalder, J., Patthey, L., Checkelsky, J.G., Ong, N.P., Fedorov, A.V., Lin, H., Bansil, A., Grauer, D., Hor, Y.S., Cava, R.J., Hasan, M.Z.: Nature **460**, 1101 (2009)
9. Zhang, H., Liu, C.-X., Qi, X.-L., Dai, X., Fang, Z., Zhang, S.-C.: Nature Phys. **5**, 438 (2009)
10. Hsieh, D., Qian, D., Wray, L., Xia, Y., Hor, Y.S., Cava, R.J., Hasan, M.Z.: Nature **452**, 970 (2008)
11. Hor, Y.S., Williams, A.J., Checkelsky, J.G., Roushan, P., Seo, J., Xu, Q., Zandbergen, H.W., Yazdani, A., Ong, N.P., Cava, R.J.: Phys. Rev. Lett. **104**, 057001 (2010)
12. Kriener, M., Segawa, K., Ren, Z., Sasaki, S., Ando, Y.: Phys. Rev. Lett. **106**, 127004 (2011)
13. Liu, Z., Yao, X., Shao, J., Zuo, M., Tan, L., Zhang, C., Zhang, Y.: J. Am. Chem. Soc. **137**, 10512 (2015)
14. Shruti, V.K., Maurya, Neha, P., Srivastava, P., Patnaik, S.: Phys. Rev. B **92**(R), 020506 (2015)
15. Wang, Z., Taskin, A.A., Frolich, T., Barden, M., Ando, Y.: Chem. Mater. **28**, 779 (2016)
16. Lawson, B.J., Corbae, P., Li, G., Yu, F., Asaba, T., Tinsman, C.: Phys. Rev. B. **94**, 041114 (2016)
17. Hor, Y.S., Checkelsky, J.G., Qu, D., Ong, N.P., Cava, R.J.: J. Phys. Chem. Solids **72**, 572 (2011)
18. Scherrer, S., Scherrer, H.: CRC Handbook of Thermoelectrics edited by D. M. Rowe. CRC Press (1995)
19. Tang, H., Liang, D., Qiu, R.L.J., Gao, X.P.A.: ACS Nano **5**, 7510 (2011)
20. Goldsmid, J.H., Douglas, R.W.: J. Appl. Phys. **5**, 458 (2002)
21. Yue, Z.J., Wang, X.L., Dou, S.X.: Appl. Phys. Lett. **101**, 152107 (2012)
22. Yan, Y., Wang, L.-X., Yu, D.-P., Liao, Z.-M.: Appl. Phys. Lett. **103**, 033106 (2013)
23. Wang, Z.H., Yang, L., Li, X.J., Zhao, X.T., Wang, H.L., Zhang, Z.D., Gao, X.P.A.: Nano Lett. **14**, 6510 (2014)
24. Zhang, S.X., McDonald, R.D., Shekhar, A., Bi, Z.X., Li, Y., Jia, Q.X., Picraux, S.T.: Appl. Phys. Lett. **101**, 202403 (2012)
25. Awana, G., Sultana, R., Maheshwari, P.K., Goyal, R., Gahtori, B., Gupta, A., Awana, V.P.S.: J Supercond. Nov. Magn. **30**, 853 (2017)
26. Sultana, R., Neha, P., Goyal, R., Patnaik, S., Awana, V.P.S.: J. Magn. Mag. Mater. **428**, 213 (2017)
27. Dutta, P., Bhoi, D., Midya, A., Khan, N., Mandal, P., Samatham, S.S., Ganesan, V.: Appl. Phys. Lett. **100**, 251912 (2012)
28. Irfan, B., Chatterjee, R.: Adv. Mater. Lett. **7**, 886 (2016)
29. Yuan, J., Zhao, M., Yu, W., Lu, Y., Chen, C., Xu, M., Li, S., Loh, K.P., Bao, Q.: Materials **8**, 5007 (2015)
30. Vilaplana, R., Perez, D.S., Gomis, O., Manjon, F.J., Gonzalez, J., Segura, A., Munoz, A., Hernandez, P.R., Gonzalez, E.P., Borras, V.M., Sanjose, V.M., Drasar, C., Kucek, V.: Phy. Rev. B **84**, 184110 (2011)
31. Kim, Y., Chen, X., Wang, Z., Shi, J., Miotkowski, I., Chen, Y.P., Sharma, P.A., Sharma, A.L.L., Hekmaty, M.A., Jiang, Z., Smirnov, D.: Appl. Phys. Lett. **100**, 071907 (2012)
32. Moudler, J.F., Stickle, W.F., Sobol, P.E., Bomben, K.D.: Handbook of X-ray Photoelectron Spectroscopy. Perkin-Elmer, Eden Prairie (1992)
33. Zhang, G., Qin, H., Teng, J., Guo, J., Guo, Q., Dai, X., Fang, Z., Wu, K.: Appl. Phys. Lett. **95**, 053114 (2009)